THE JOURNAL OF PHYSICAL CHEMISTRY B

Article

pubs.acs.org/JPCB

Spectroscopy and Kinetics of Tyrosinase Catalyzed *trans*-Resveratrol Oxidation

Alicia G. Gonzálvez,[†] Ángel González Ureña,[†] Richard J. Lewis,[†] and Gert van der Zwan*[,‡]

[†]Instituto Pluridisciplinar, Universidad Complutense de Madrid, Paseo Juan XXIII 1, 28040 Madrid, Spain

[‡]Biomolecular Analysis and Spectroscopy Laser Laboratory, Vrije Universiteit, de Boelelaan 1083, 1081HV Amsterdam, The Netherlands

Supporting Information

ABSTRACT: The spectroscopy and kinetics of the tyrosinase catalyzed *trans*-resveratrol oxidation were investigated by measuring both UV−vis absorption spectra over the 200−500 nm range and Raman spectra over the 600−1800 cm^{-1} region. Room temperature UV−vis absorption spectra, as a function of time, showed the presence of two isosbestic points located at λ_1 = 270 nm and λ_2 = 345.5 nm delimiting two different regions: the reactant region around 300 nm, where the absorption decreased with time, and the product region over the low wavelength (λ < 260 nm) and high wavelength (λ > 390 nm) wavelength zone in which the absorption increased with time until, in both cases, constant values were achieved. A first-order kinetics was deduced with a rate coefficient of k_1 = (0.10 ± 0.001) min^{-1}, which turned out to be independent of substrate concentration over the 50−5 μM range; a feature that was rationalized by invoking the limiting case of the Michaelis−Menten scheme appropriate for substrate concentration much lower than the respective Michaelis constant. The observation of the distinct resonance enhanced Raman lines, specifically those peaking at 830 cm^{-1}, 753 cm^{-1}, and 642 cm^{-1} together with their time evolution, permitted us to gain insight into some crucial features and steps of the catalytic reaction. Namely, that the formation of the so-called *trans*-resveratrol and tyrosinase ^{S}P complex with its O−O bridge plays a crucial role in the first steps of this enzymatic reaction and that the hydroxylation of the ortho C−H bond of the *trans*-resveratrol OH group occurs *after* O−O bond cleavage in the tyrosinase active site. The present study makes clear that a class of potential inhibitors of tyrosinase can be found in compounds able to bind the two Cu (II) ions of the enzyme bidentate form.

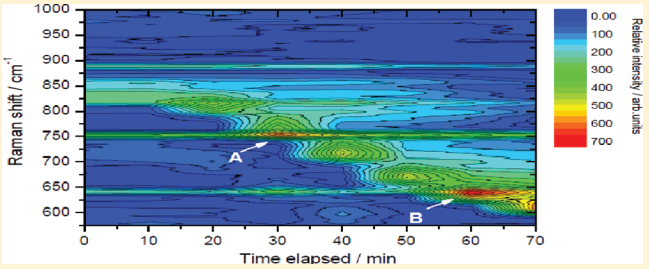

INTRODUCTION

Tyrosinase (EC1.14.18.1), hereafter denoted by ty, is an important protein in the fields of medicine, agriculture and industry,[1−9] and the cosmetic industry.[2] It is present in fruits, vegetables, and mushrooms and plays an essential role in the fruit browning mechanism as well as in mammalian skin pigmentation, due to its crucial activity in the synthesis of melanin pigments.

The catalytic activity of ty is well documented to be associated with its active site formed of two copper atoms, which is responsible for the hydroxylation of phenols to catechols and the oxidation of catechols to quinones.[1,3,8,9]

The ty enzyme can be found in several isoforms,[3] namely, oxidized (oxyty, E_{oxy}), met (metty, E_{met}) and reduced (deoxyty, E_{deoxy}); these forms are illustrated in Figure 1.

The oxidized form (E_{oxy}) contains two tetragonal Cu(II) atoms, each coordinated by two strong equatorial and one weaker axial histidine N_{His} ligand, while an exogenous oxygen molecule is bound as peroxide bridging the two Cu centers. It was firmly established already in 1938 that E_{deoxy} consists of a bicuprus structure.[4] Finally, the met form (E_{met}), like the oxy form, has two tetragonal copper(II) ions coupled through an

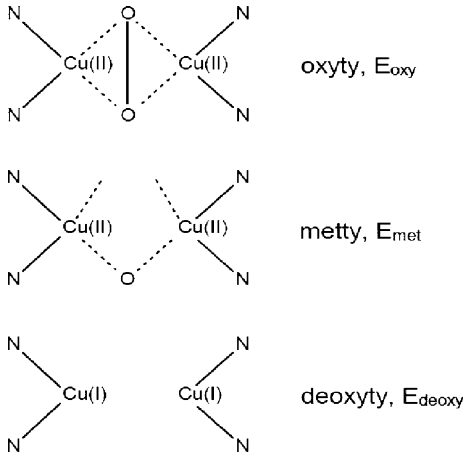

Figure 1. Forms of the tyrosinase enzyme ty. Top to bottom: oxidized (oxy, E_{oxy}), met (met, E_{met}), and reduced (deoxy, E_{deoxy}).

Received: October 11, 2011
Revised: February 2, 2012
Published: February 2, 2012

dx.doi.org/10.1021/jp209753q | *J. Phys. Chem. B* 2012, 116, 2553−2560

endogenous bridge, although hydroxide exogenous ligands other than peroxide are bound to the copper site.[3,8]

Studies of the structure and spectroscopy of copper−dioxygen complexes in general (and that of ty in particular) have attracted much attention in recent years due to their potential relevance to biochemical systems and synthetic catalysis.[3,8] It was not until the experimental determination of their crystallographic structures[1,3,9] that it became amenable to study at the atomic level. Nevertheless, even today a deep knowledge of the reaction mechanisms of ty with many antioxidants remains unclear.

However, *trans*-resveratrol (3,5,4′-trihydroxystilbene), hereafter denoted by t-res, is a well-known antioxidant compound naturally produced by vines and other plants as a self-defense agent acting against a pathogenic attack, which has recently attracted increased interest as a health-promoting agent due to its antiplatelet, antioxidant, anti-inflammatory, estrogenic, cardioprotective, and cancer chemopreventive properties. As such, it has been widely reviewed.[10−16]

The oxidation of phenolic compounds catalyzed by ty was studied extensively by several groups.[1,3,8] Thus, it is well-known that ty upon O_2 binding exhibits a characteristic side-on bridging peroxodicopper(II) active center forming the core of the so-called P intermediate[1] to which the phenolic substrate binds directly and is, subsequently, hydroxylated via an electrophilic aromatic substitution. While the capability of oxyty to hydroxylate the ortho C−H bond is well documented[1,3,8] to occur via the mentioned P intermediate, little is known on the intermediates beyond P. This lack of information constitutes one of the motivations for the present investigation.

In addition, despite the large number of studies on the catalytic activity of ty with a rich variety of substrates, including phenols, there are very few using t-res. Among them, we can mention the t-res degradation by a novel ty extracted from Carignan grape juice carried out by Gilly et al.[17] and by the ty inhibition by t-res using UV−vis spectroscopy whose main emphasis was to investigate the t-res potentiality as a bioactive agent for cosmetics.[2] In none of these latter investigations was a detailed spectroscopic analysis presented based on highly sensitive techniques such as resonant Raman spectroscopy and, consequently, no detailed assessment on the different reaction steps was experimentally evidenced.

From the kinetic point of view, there is no information on how fast t-res oxidation is and whether the catalytic reaction occurs via any reaction intermediate. For the latter possibility, it would be interesting to know the structure of such intermediate and the role played by the enzyme active center and the t-res OH groups.

As the catalytic oxidation reaction requires the presence of O_2, a full understanding of the enzymatic reaction will also require to unravel the particular O_2 binding to the active center mediating the substrate (t-res) oxidation. In other words, one needs to know if the oxidation reaction proceeds via a peroxide O−O bridge, or any other related structure, bound to the dicopper center of the enzyme. For the latter option, it would be interesting to determine whether the O−O cleavage takes place during or before the hydroxylation of the C−H bond of the t-res.

Even accepting the working hypothesis of the peroxide intermediate formation as the initial configuration of the ty active center, this information is insufficient to fully understand the subsequent mechanistic steps leading to the final oxidation products. Indeed, a proper answer to the above questions would be of a great value not only from a fundamental point of view but, especially, for the design of specific ty inhibitors.

To reach the objectives cited above, the present investigation recorded both UV−visible absorption and Raman spectroscopic data as a function of the time elapsed following ty and t-res mixtures under distinct experimental conditions. We anticipate that the observation of the time evolution of several UV−visible absorption and Raman signatures associated to distinct intermediates formed during the catalytic reaction allowed us to unravel the mechanism of this important reaction.

EXPERIMENTAL SECTION

Reagents and Standards. Ty extracted from mushrooms and t-res samples were purchased from Sigma Aldrich, both with a stated purity of 99%. Phosphate buffered saline (PBS) of neutral pH was used as the solvent to prepare all samples. The standard samples used in this work were solutions of 1:1 mixtures of 700 pM ty and 100 μM t-res, as this was determined to be the optimal concentration ratio for both the UV−visible and Raman spectroscopy measurements. In order to investigate the reaction dependence on the t-res concentration, the kinetics was repeated using different substrates, i.e., t-res concentration over the 50−5 μM range.

UV−Visible Spectroscopy. The UV−visible spectroscopic measurements were carried out using a Perkin-Elmer Lambda 40 spectrophotometer, and the absorption was measured in the range 200−500 nm, with one measurement every 30 s during a total measurement period of 70 min.

Raman Spectroscopy. The Raman spectroscopic measurements were performed using a custom-built Raman microscope in a backscattering configuration whose main details have been published elsewhere.[18,19] In summary, the Raman microscope consists of a Zeiss D7082 microscope (with a 40× objective, numerical aperture 0.85, and working distance of 2 mm) coupled to an Andor Shamrock SR-303i single monochromator equipped with a 2400 lines/mm holographic grating and an Andor Newton DU970N CCD camera. A Coherent Innova 300c continuous wave krypton ion (Kr^+) laser with a principal emission wavelength of 413.1 nm was employed for excitation, and the Rayleigh scattered light was removed by an Omega Optical Third Millennium long pass edge filter. A 1 mm diameter capillary was used to contain the samples, and during all measurements, this capillary was kept spinning to minimize local heating.

The standard samples were prepared to a total volume of 100 μL and immediately drawn into the capillary. Laser power on the sample was an approximately constant 5mW. One measurement was made every 10 min for 70 min, with each measurement consisting of the binning of 15 individual 10 s exposures. To ensure reproducible results, each measurement was repeated five times.

RESULTS AND DATA ANALYSIS

The main body of results presented in this section are divided between the UV−visible absorption and Raman spectroscopic data for individual analysis and discussion. As already mentioned, the data under investigation in each case is presented during a total measurement period of 70 min.

UV−Visible Absorption Spectra. Figure 2 displays, in contour plot form, the UV−visible absorption in the 200−500 nm region as a function of time. Inspection of this figure

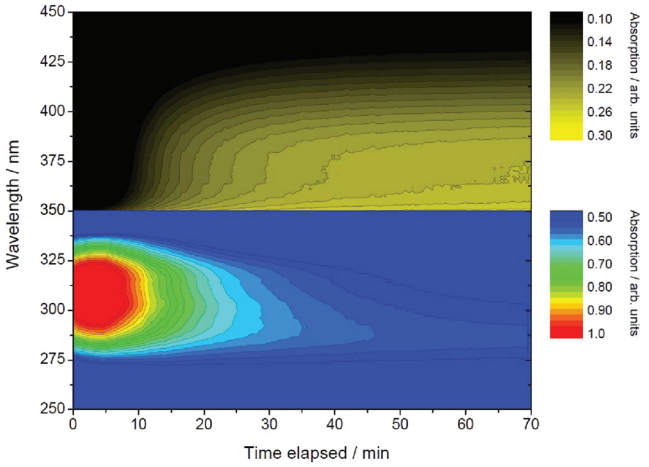

Figure 2. Contour absorption mapping. Contour mapping representation of the absorption data (arb. units) measured every thirty seconds of the t-res−ty mixture. Although the absorption signal range for the upper and lower panels are different, they use the same arbitrary units.

indicates the presence of two spectral regions showing a different time evolution. While the absorption near 300 nm decreases with time, the absorption in the longer wavelength regions at approximately 400 nm increases with time. In both cases, the absorption approaches steady values for $t > 50$ min.

Repeated scans of the UV−vis spectral evolution with the reaction time are also shown in the two-dimensional plot depicted in Figure 3 where, in addition to the mentioned

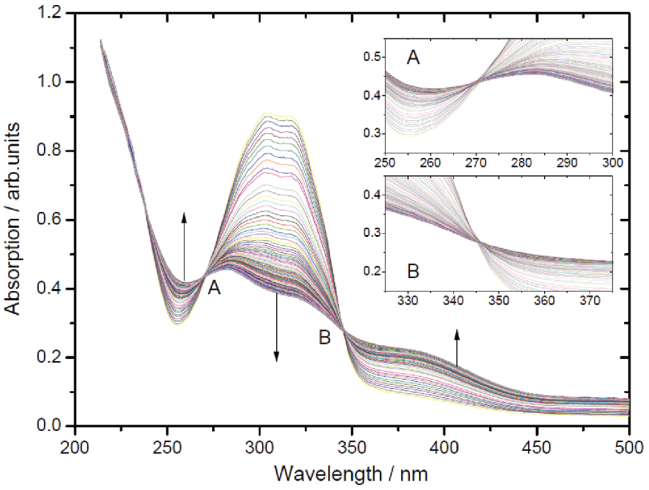

Figure 3. Repeated scans of UV−vis absorption spectra over the 200−500 nm range during the measurement period of 70 min. Different colors represent the individual measurements taken every 30 s, and the arrows indicate the temporal evolution of the indicated regions. Notice the presence of two isosbestic points around 270 nm and 345.5 nm. Two zoomed-in insets provide a clearer view of these two points.

temporal evolution, two isosbestic points (also shown in the respective insets for a better display) located at $\lambda_1 = 270$ nm and $\lambda_2 = 345.5$ are clearly noticed.

Two cross-sections of the absorption contour map at 304 and 400 nm are shown in Figure 4 to more clearly distinguish the kinetic behavior. The cut at 304 nm represents the time evolution of the t-res consumption, and a simple exponential

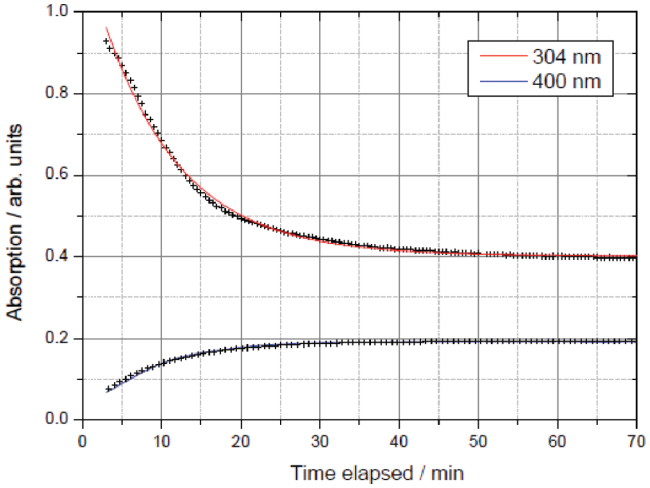

Figure 4. Temporal evolution of absorption at 304 nm (red, top) and 400 nm (blue, bottom). UV−visible spectra done every 30 s during the measurement period of 70 min. The absorption data is represented in both cases by crosses and the fitted exponential models as solid colored lines.

decay model of the concentration can be fitted to these data, i.e.,

$$[\text{t-res}] = [\text{t-res}]_0 \exp(-k_1 t)$$

The cut at 400 nm represents product (quinone, P) appearance, which can be represented by the particular exponential growth model

$$[\text{P}] = [\text{P}]_0(1 - \exp(-k_1 t))$$

Note that models use k_1 as the rate coefficient; this is to be expected from the reaction kinetics, and the best-fit value was found to be $k_1 = (0.10 \pm 0.01)$ min^{-1}.

The kinetic experiment was repeated changing the t-res concentration over the 50−5 μM range. In all cases and even at concentrations as low as 5 μM, the temporal evolution of the reactants and product absorption could be fitted by the same exponential law used earlier, and more interestingly, within the experimental error of our experiments $\varepsilon = 10\%$, the same value of k_1 was found. In other words, under the experimental conditions employed in the present study, the kinetic of the t-res oxidation can be described by a first order kinetic (see further below for a discussion on this point) with respect to substrate concentration.

Raman Spectra. A contour map of the total Raman signal is displayed in Figure 5 as a function of the Stokes Raman shift in the 600−1800 cm^{-1} region, and the elapsed time since the reaction mixture was prepared.

Although the two-dimensional representation of the time evolution of the Raman spectrum is instructive, one is hampered in its interpretation due to the fact that the Raman lines are superimposed upon an uneven background of (primarily) fluorescence. In spite of the fact that it is impossible to completely separate the Raman signals from the background, a high degree of separation is nevertheless possible by application of a suitable postacquisition software filter.

In this study, a modified version of the well-known rolling circle filter (RCF) has been applied. The basic RCF approach was reported in 2006 by Brandt et al.,[20] and in that work, the RCF is utilized as a high-pass filter, whereby a rigid circle with a radius larger than the Raman line widths (but less than the

dx.doi.org/10.1021/jp209753q | J. Phys. Chem. B 2012, 116, 2553−2560

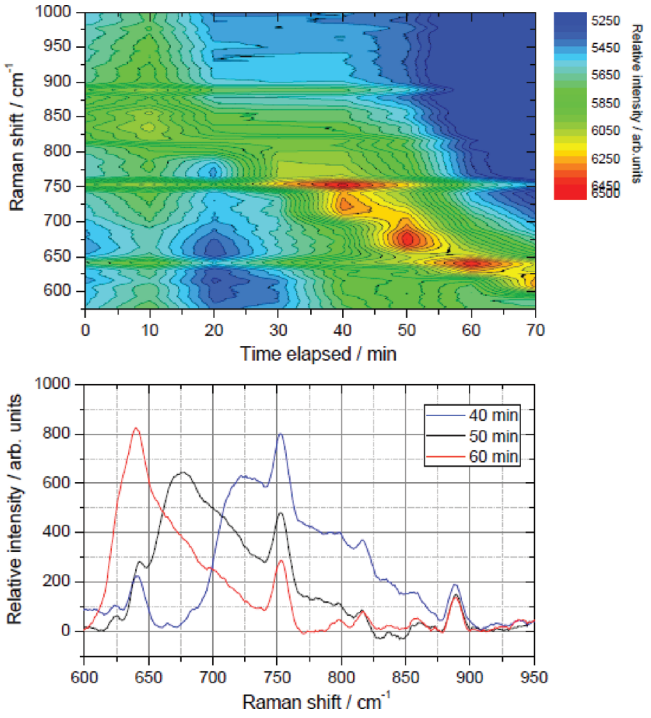

Figure 5. Fluorescence and Raman data. Top: contour map of the raw data measured every 10 min of the t-res−ty mixture. Bottom: total fluorescence and Raman signal at different times elapsed since the reactants were mixed, as indicated.

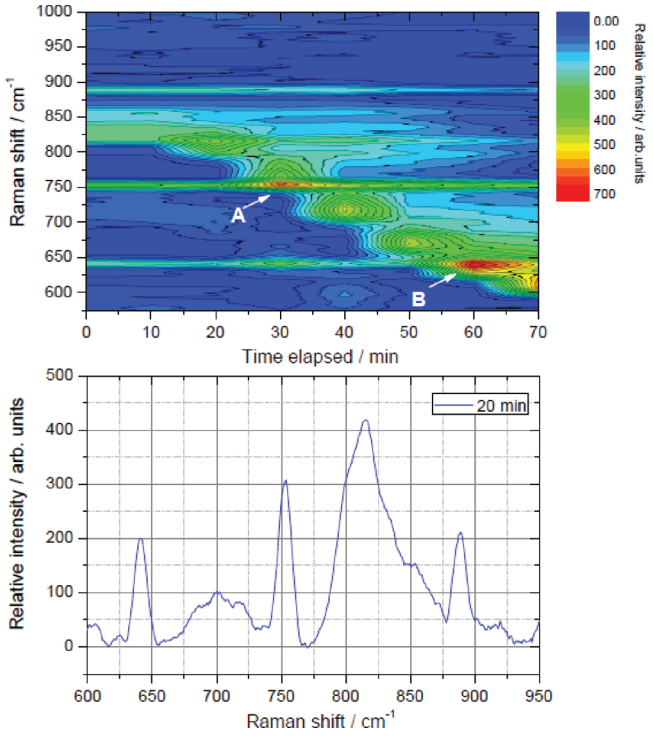

Figure 6. Top: contour map of the Stokes Raman spectrum with respect to time. The Raman data was isolated from the background fluorescence by applying the RCF methodology described in the text to the data shown in graph 3. Color relative intensity scale (arb. units) at the right. Notice the distinct peaks manifested at different wavenumbers and times. The location of the two main reaction intermediates are marked in capital white letters as A and B. See text for a discussion on this matter. Bottom: vertical cut of the contour map at 20 min. Notice the presence of the four peaks at 889 cm^{-1}, 830 cm^{-1}, 753 cm^{-1}, and 642 cm^{-1}.

fluorescence variation) is rolled underneath a spectral trace. The locus of the top of the circle is (after adding the average of the background noise level) used as a model of the background. A simple subtraction of this model then yields a Raman spectrum with a significantly reduced background.

This approach, while simple in concept and application, is insufficient for our purposes since we wish to retain the fluorescence model as well as the Raman spectrum. Further, since the Raman features we are interested in are not much narrower than features in the fluorescence, it is not possible to simply select a circle radius that provides a reliable degree of separation of the fluorescence (the circle locus) and the Raman features (the residue).

Our modification is to couple a Savitzky−Golay (SG) smoothing filter to the model of the locus. By coupled we mean that the number of points included in the SG filter window is equal to the radius of the circle rolled underneath the spectral trace. In this way, an appropriate level of smoothing is applied to the locus, which greatly reduces the leakage of Raman features into the model of the fluorescence, and conversely reduces the degree to which the shape of the Raman features themselves are distorted by the circle having rolled into the same features. A third-order polynomial was used for the SG filter model throughout.

The contour map of the Raman signal obtained by applying the method briefly described above is shown in Figure 6. Comparison of this data set with the original raw data contour map makes evident the higher degree of separation of the filtered Raman signals from the background, which even permits the identification of a clear series of peaks at different Raman shifts and reaction times.

To reinforce the association of these Raman signals to the induced reaction, a typical Raman spectrum at t = 20 min after the ty and t-res mixture was prepared (i.e., a vertical cross-section of Figure 6 is shown in the bottom of the figure where several peaks are noticeable, namely, at 889 cm^{-1}, 830 cm^{-1}, 753 cm^{-1}, and 642 cm^{-1}.

Interestingly, these above-mentioned Raman lines are absent from spectra of pure t-res, pure ty, ty bubbled with pure oxygen, and a ty and t-res mixture bubbled with pure nitrogen (spectra not shown), which clearly indicates that the Raman signals originate solely from the ty and t-res mixture in the presence of oxygen.

As pointed out earlier, a direct analysis of the Raman data depicted in the contour map of graph 5 indicates the presence of several intermediates such as one peaking at 754 cm^{-1} and 30 min and another peaking at 642 cm^{-1} and 50 min. The kinetic evolution of these Raman signatures, i.e., the corresponding horizontal cuts, is illustrated in Figure 7, and their role in the enzymatic reaction mechanism will be discussed in the next section.

DISCUSSION

The oxidative degradation of t-res catalyzed by lipoxygenase-1 (LOX-1) studied by Pinto et al.[21] showed the presence of two distinct temporal behaviors, a decrease of the absorption near the 300 nm region and a continuous increase in absorption at 250 nm and in the region of 375−395 nm, as well as the occurrence of two isosbestic points at 275 nm and 369 nm. The latter feature is often interpreted as only two species are

dx.doi.org/10.1021/jp209753q | J. Phys. Chem. B 2012, 116, 2553−2560

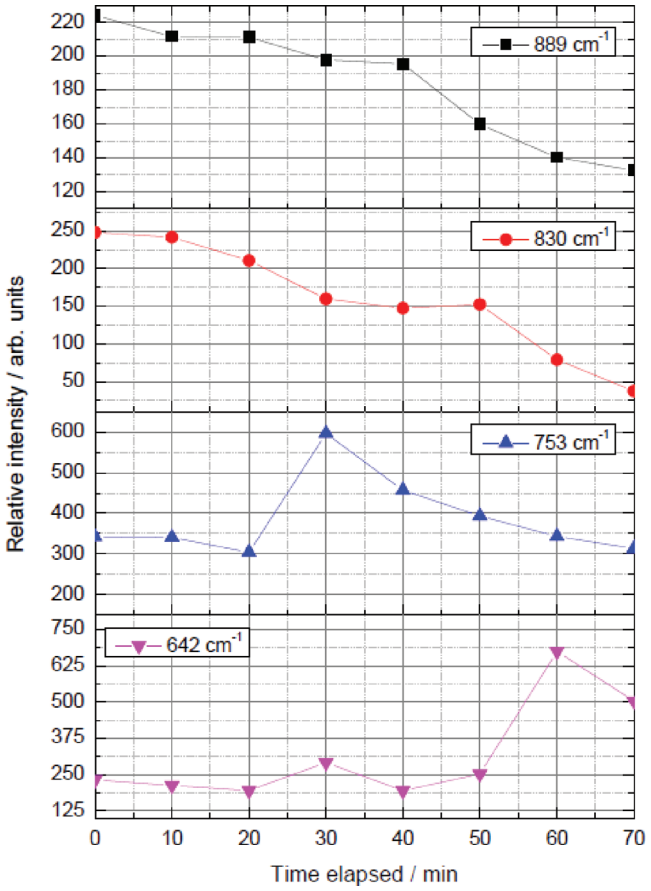

Figure 7. Temporal evolution of Raman signal. Horizontal cuts of the Raman data shown in Figure 6 at the wavenumbers of 889 cm^{-1}, 830 cm^{-1}, 753 cm^{-1}, and 642 cm^{-1}.

involved in the oxidative processes. Nevertheless, one could not rule out the presence of additional products with negligible absorption in the UV−vis range.

It is then remarkable the overall similarity of the absorption spectra as well as their time of evolution between the present t-res plus ty reaction and the mentioned t-res oxidative degradation catalyzed by LOX-1, which seems to suggest the formation of similar oxidation products in the course of the catalytic reactions.

It is well accepted that *o*-quinones are the primary products of the enzymatic oxidation of phenolic substrates by ty;[22,23] compounds that, in general, are unstable and can be separated according to their UV−vis spectra[22] into two main categories: colored compounds (λ_{max} = 294−324 nm) and colorless compounds (λ_{max} = 264, 280, or 290 nm).

The observation (see Figure 4) that the absorption at 304 nm decreases with time, that beyond 50 min remains constant and does not reach a zero value, may be an indication of the formation of these colored reaction products. Further below, we will see how the presence of these colored products does not affect the rate coefficient determination of the t-res oxidation.

The fact that both the t-res decay and the product formation data could be fitted by an exponential decay and growth law with the same rate coefficient suggests the presence of a first-order kinetic. Unfortunately, the body of data available is not sufficient to clearly assess the detailed kinetic mechanism of the reaction under study. As described in the Supporting Information, under the employed experimental conditions, several reaction schemes lead to a first-order rate equation for both product formation and reactant consumption. Among them, we like to mention (i) the consecutive reaction figure $A \rightarrow B \rightarrow C$ providing that the first step is the rate limiting step, i.e., if $k_1 \ll k_2$ and (ii) the Michaelis−Menten mechanism given by $E + S \rightarrow ES \rightarrow P + S$, where S stands for substrate (t-res in the present case), E for ty, and P for product.

In the Supporting Information (eq 14), it is shown that when the substrate concentration is much lower than the Michaelis constant, k_m, i.e., $[S] \ll k_m$, the kinetics are first-order in substrate concentration. In the study carried out by Gilly et al,.[17] it was found that t-res was significantly degraded by a novel ty prepared from Carignan grapes. These authors also reported for the respective reaction a k_m value of 350 μM.

Although our conditions, especially those concerning the ty origin, are not the same as those used in ref 17, we should note that the requirements for first-order kinetics are easily obeyed in view of the employed t-res 50−5 μM concentration range values; clearly lower than that of the Michaelis constant cited above.

We would like then to emphasize that the main objective of the present investigation is to gain insight into the distinct intermediates on the titular reaction from both the spectroscopic assignments and the time evolution of the different Raman signatures experimentally observed. This matter is now discussed below.

The four experimental Raman lines observed in the present investigation, at 889 cm^{-1}, 830 cm^{-1}, 753 cm^{-1} and 642 cm^{-1}, are compared in Table 1 with well-known Raman features of 2:1 Cu/O_2 complexes reported in the literature.[1,3]

With respect to the moderately intense peak at 889 cm^{-1}, it should be noted that this shift has been clearly assigned to the O−O stretching of the hydroperoxo−copper complex by Solomon and co-workers.[3,6] These authors demonstrated how this mode is strongly enhanced by the 25 00 cm^{-} absorption band of the $[Cu(UN-O-)OOH)](PF_6)_2$ complex.[3,6] On the basis of these findings, we have assigned the observed 889 cm^{-1} line to the Cu(OOH)Cu unit of the ty−t-res complex, which likely could be resonantly enhanced by the laser excitation at 24 207 cm^{-1} (i.e., the Kr^+ laser wavelength of 413.1 nm).

Table 1. Major Observed Raman Signatures and Their Spectroscopic Assignments[a]

Raman shift (cm^{-1})[b]	spectroscopic assignments[b]	Raman shift (cm^{-1})[c]	spectroscopic assignments[c]
889	(Cu−OOH−Cu) unit in hidroxo−peroxo−copper complex formed with t-res and ty (O−O stretching)	889	(Cu−OOH−Cu) unit; other hidroxo−peroxo−copper formed with ty and different ligands[24]
830	^{T}P complex formed with t-res and ty (O−O stretching)	830	^{T}P ty complexes with different ligands (O−O stretching)[1,8]
753	μ−η^2:η^2−peroxodicopper(II) ^{S}P t-res−ty complex (O−O stretching)	730−760	distinct ^{S}P complexes[1]
642	[Cu−O(φ)−Cu] moiety ν_S and ν_{AS} vibrational modes	643	[Cu−O(Ph)−Cu] moiety ν_S and ν_{AS} vibrational modes[8,24]

[a]See Figure 9 for the structure of radical φ. [b]From the present work. [c]From specified references.

dx.doi.org/10.1021/jp209753q | J. Phys. Chem. B 2012, 116, 2553−2560

However, it should be noted that the Raman signatures centered at 830 cm^{-1}, 740 cm^{-1}, and 600 cm^{-1} are well documented to be associated to the presence of the so-called ^{T}P, ^{S}P, and O 2:1 Cu/O_2 complex intermediates, respectively, and whose main structures have been already described in the literature.[1,3,8]

There exist a considerable number of spectroscopic studies of the $\mu-\eta^2:\eta^2-$peroxodicopper(II) complexes (the so-called ^{S}P complexes), generally with tetradentate ligands. The most common spectroscopic features of such complexes are directly related to the side-on peroxide binding mode. In general, the absorption spectra of these ^{S}P species exhibit[25] a high-energy charge-transfer (CT) band (340−380 nm, ε = 18 000−25 000 M^{-1} cm^{-1}) and a weaker lower energy CT band (510−560 nm, ε = 1000 M^{-1} cm^{-1}). Of relevance to the present investigation is the study carried out by Solomon and co-workers[8] on the reaction of a $\mu-\eta^2:\eta^2-$peroxodicopper(II) species with a 2,4-di-*tert*-butylphenolate. The authors observed several intermediates exhibiting distinct absorption bands, specifically a ∼23 900 cm^{-1} band (ε = 18 000 M^{-1} cm^{-1}), i.e., centered at 418 nm, a wavelength close to the laser principal emission wavelength of 413.1 nm employed in the present work. This latter feature together with the use of ty and t-res (a polyphenol) as reactants provided both the spectroscopic and functional similarities required for the (resonant) Raman investigation on the enzymatic t-res oxidation performed in the present work.

In general, the resonant Raman (rR) spectra[1,2] of the ^{S}P intermediates show a low-energy O−O stretching vibration at 730−760 cm^{-1}. This lower value compared to that of the normal peroxide ion (ca. 830 cm^{-1}) is thought to result from back-bonding from Cu(II) orbitals into the orbital σ^* of the peroxide ion;[25] an electron transfer that not only weakens the O−O bond but also influences its cleavage.

In this view, the experimentally observed lines at 830 cm^{-1} and 753 cm^{-1} could be assigned to the enhanced resonant Raman lines of the so-called ^{T}P and ^{S}P 2:1 Cu/O_2 complex intermediates, respectively, formed in the ty−t-res reaction.

Concerning the observed Raman line at 642 cm^{-1}, it should be noted that experimental measurements and DFT calculations carried out in the work of Op't Holt[8] showed that vibrations at 648 cm^{-1}, 589 cm^{-1}, and 560 cm^{-1} correspond to modes of the Cu_2O_2 core. Moreover, a detailed study carried out by Root et al.[24] assigned the 643 cm^{-1} peak of the Cu_2(OPh, Ph = phenyl) complex either to the ν_S (Cu−O(Ph)−Cu) or to the ν_{AS} (Cu−O(Ph)−Cu) vibrational mode. Likewise, on the basis of this analysis, we have assigned our experimentally observed 642 cm^{-1} peak either to the ν_S (Cu−O(φ)−Cu) or the ν_{AS} (Cu−O(φ)-Cu) vibrational mode. See the representation of the reaction mechanism in Figure 8 and Table 1 for the spectroscopic assignments. See also Figure 9 for a definition of the φ radical.

In addition to the spectroscopic assignment of the observed Raman signatures, the time evolution of these signatures is of major relevance for the present investigation. As illustrated in Figure 7, the following main kinetic features are noticeable: (i) a rather continuous decline with time of both the 889 cm^{-1} and 830 cm^{-1} signal intensities and (ii) an initial rise and subsequent decline of the 753 and 642 cm^{-1} line intensities, peaking at 30 min and 60 min, respectively.

As for the main reaction pathway of the t-res oxidation catalyzed by the ty, it is important to note that based on the crystal structure of ty as determined by Matoba et al.,[9] the catalytic conversion of monophenol to the corresponding

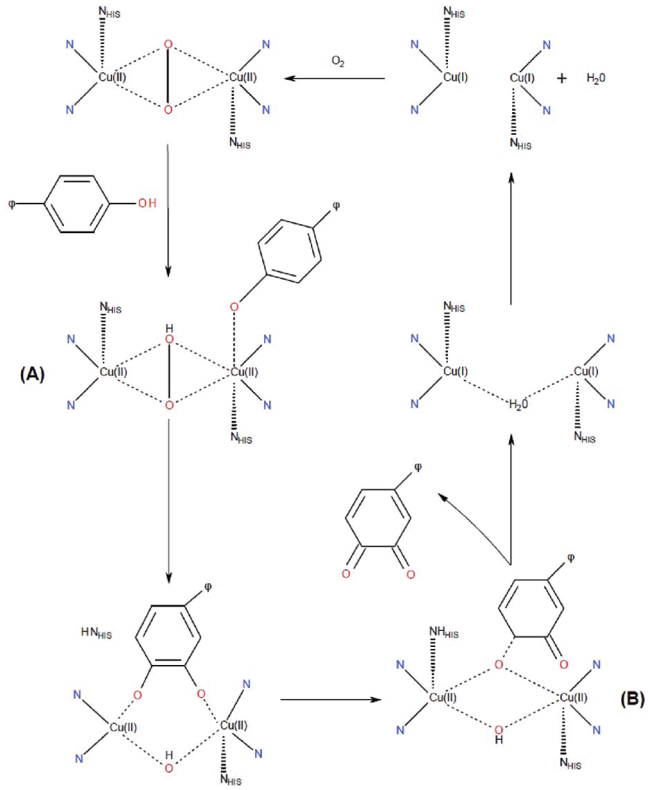

Figure 8. Suggested reaction mechanism for the t-res oxidation induced by the ty. The main reaction intermediates are labeled as A and B as also indicated in Figure 6. The three histidine groups for each copper atom are denoted by N. To emphasize some reaction steps, the histidine groups above and below the equatorial plane are labeled N_{HIS}. See Figure 9 for the definition of the radical φ.

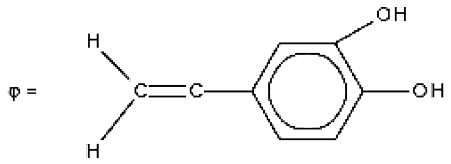

Figure 9. Structural diagram of the radical φ used as an abbreviation in Figure 8.

quinone through the ortho-diphenol formation is thought to occur via the intermediate formation of a $\mu-\eta^2:\eta^2-$peroxodicopper(II) species.

Following this mechanistic scheme together with the detailed spectroscopic information and time evolution of the observed Raman signatures obtained in the present investigation, the main steps proposed for the ty catalytic oxidation of the t-res are outlined in Figure 8. In this scheme, the first step is the action of the peroxide ion, which forms a bridge with two Cu(II) ions featuring the so-called oxy form of ty. This form acts as a base and takes a proton from the phenolic hydroxyl, while the phenolate radical binds to Cu^B just at the sixth coordinate site leading to the intermediate named A in Figures 6 and 8, which represents the ty−t-res ^{S}P complex whose main Raman line peaks at 753 cm^{-1} and 30 min.

The next step is the cleavage of the O−O bond. As it is outlined in the reaction mechanism, while an *ortho*-carbon of the t-res substrate approaches the peroxide ion, one of the two peroxide oxygens is therefore added to the *ortho*-carbon of the monophenol. As a result, the newly generated O atom of the

dx.doi.org/10.1021/jp209753q | J. Phys. Chem. B 2012, 116, 2553−2560

diphenol moiety binds to Cu^A. This intramolecular motion leads to the H54N release from its position that is likely facilitated by the H54N residue flexibility, a dynamical feature evidenced by the crystallographic study conducted by Matoba et al.[9]

Electron rearrangements in the resulting intermediate can finally form both the quinone and the deoxy form of ty. It is likely that the quinone formation involves a sequential step in which a C═O bond is formed first. Subsequently, the second C═O bond is produced and the product *o*-quinone released after ligand displacement and H54N recombination with the Cu^A(II) ion. Certainly because of the shorter Cu−Cu distance[1,9] and final H54N recombination, one may expect that the intermediate B, see the reaction scheme, would be stable enough to be detected by the resonant Raman spectroscopic technique. Support to the latter step is provided by the observation of the Raman line at 642 cm^{-1} together with its time evolution. Its intensity shows a delayed increase (see Figure 7) after the decline of the 753 cm^{-1} Raman intensity. This temporal evolution is consistent with the A to B intermediate transformation, as marked in Figures 6 and 8, whose ν_S (Cu−O(φ)−Cu) or ν_{AS} (Cu−O(φ)−Cu) vibrational modes have been assigned to the observed 642 cm^{-1} Stokes line.

The observed Raman signatures observed in the present investigation provides evidence that in the catalytic reaction, the hydroxylation of the *ortho*-C−H bond with respect to the t-res OH group occurs *after* O−O bond cleavage. In addition, it provides information about the electronic rearrangement required for the production of *o*-quinone, which seems to take place in a sequential mode whose final step involves the Cu−O(φ)−Cu core. These mechanistic features of the enzymatic catalysis, we would like to remark, have only been possible to investigate by recording the time evolution of the resonant Raman spectra.

SUMMARY AND CONCLUSIONS

This work centered its attention in the spectroscopy and kinetics of the ty catalyzed t-res oxidation by measuring both UV−vis absorption, over the 200−500 nm range, and Raman spectra over the 600−1800 cm^{-1} region in both cases during a period of 70 min since the reaction mixture is prepared.

Overall, the full set of UV−vis absorption spectra as a function of time showed the presence of two isosbestic points located at λ_1 = 270 nm and λ_2 = 345.5 nm delimiting two different regions, namely, (i) the reactant region around 300 nm (i.e., the region between the isosbestic points), where the absorption decreased with time, and (ii) the product region over the low wavelength (λ < 260 nm) and high wavelength (λ > 390 nm) zones in which the absorption increased with time until, in all cases, it approached steady values beyond 50 min.

Although no direct chemical analysis was performed to identify the nature of the reaction products, it is well-known that the phenolic oxidation leads most predominantly to the *o*-quinone formation. Indeed, the absorption spectra observed in the present investigation confirm the presence of the *o*-quinone absorption bands over the 400−430 nm range, which is also consistent with the observed isosbestic point at 375 nm.

As for the kinetics, both the t-res decay and the product formation data could be fitted by an exponential decay and growth law, respectively, with the same rate coefficient suggesting the presence of a first-order kinetics.

The experimentally deduced rate coefficient value was k_1 = (0.10 ± 0.01) min^{-1} and, under the employed experimental conditions, turned out to be independent of the substrate concentration over the 50−5 μM range; a feature that was rationalized by invoking the limiting case of the Michaelis−Menten scheme, appropriate when the substrate concentration is much lower than the respective Michaelis constant.

One of the most relevant aspects of the present investigation is the insight gained into the reaction mechanism of the titular reaction, i.e., the main steps and the identification of spectroscopic features associated with the presence of several intermediates that has been only possible by using the powerful resonant Raman technique.

The formation of different reaction intermediates whose absorption bands, most likely associated to the charge transfer processes, were resonant or near resonant to the employed laser excitation energy making possible the observation of their enhanced Raman signatures, that otherwise would have been absent. As a result, it led to the vibration mode assignment of the t-res−ty complex intermediate reactive centers formed in the course of the catalytic reaction; a crucial piece of information that was not possible to extract solely from the absorption spectra confirming the great sensitivity of the resonant Raman technique used in the present work.

Indeed, the observation of the distinct Raman lines, specifically those peaking at 830 cm^{-1}, 753 cm^{-1}, and 642 cm^{-1} together with their time evolution, allowed us to assess the main features and steps of the catalytic reaction.

The time evolution of the Raman signatures observed in the present investigation addresses the dynamical interaction of the enzyme tyrosinase with the antioxidant t-res. Thanks to this information, it was possible to outline a detailed mechanism for the titular reaction in which the following main steps were established: (i) the formation of the t-res−ty ^SP complex with its O−O bridge plays a crucial role in the first steps of this enzymatic reaction. A reaction intermediate has been observed whose main resonant Raman signature has been observed at 753 cm^{-1} and assigned to the weakened O−O stretching of a μ−η^2:η^2−peroxodicopper(II) species featuring the ty−t-res ^SP complex; (ii) the hydroxylation of the ortho C−H bond of the t-res employs one of the O atoms from the peroxide bridge and occurs *after* O−O bond cleavage in the ty active center; (iii) the final step of the enzymatic reaction that seems to involve an intermediate complex whose resonantly enhanced ν_S (Cu−O(φ)−Cu) or ν_{AS} (Cu−O(φ)-Cu) vibrational modes were assigned to the observed 642 cm^{-1} Raman Stokes line.

Finally, one should point out the crucial role of the bidentate form of the oxyty in the catalytic reaction, in particular, in the quinone formation. Obviously, potential inhibitors of tyrosinase must be able to bind to the two Cu(II) ions of the bidentate form.

ASSOCIATED CONTENT

Supporting Information

Description of some kinetic models appropriate for the analysis of the results. This material is available free of charge via the Internet at http://pubs.acs.org.

AUTHOR INFORMATION

Corresponding Author

*E-mail: g.vander.zwan@vu.nl.

Notes

The authors declare no competing financial interest.

■ ACKNOWLEDGMENTS

This research received financial support from the Spanish Ministerio de Ciencia e Innovación (MICINN, grant CTQ2007-61749), the Government of the Madrid Region, and from the Complutense University of Madrid. A.G.G. acknowledges both a FPI fellowship and a visiting fellowship under the "Estancia Breves" programme of the MICINN of Spain at Amsterdam University.

■ REFERENCES

(1) Mirica, L. M.; Ottenwaelder, X.; Stack, T. D. P. *Chem. Rev.* **2004**, *104*, 1013−1046.
(2) Bernard, F.; Berthon, J.-Y. *Int. J. Cosmet. Sci.* **2000**, *22*, 219−226.
(3) Solomon, E. I.; Sundaram, U. M.; Machonkin, T. E. *Chem. Rev.* **1996**, *96*, 2563−2606.
(4) Kubowitz, F. *Biochemistry* **1938**, *299*, 32−57.
(5) Sánchez-Ferrer, A.; Rodríguez-López, J. N.; García-Cánovas, F.; García-Carmona, F. *Biochim. Biophys. Acta* **1995**, *1247*, 1−11.
(6) Solomon, E.; Lowery, M. *Science* **1993**, *259*, 1575−1581.
(7) Wilcox, D. E.; Porras, A. G.; Hwang, Y. T.; Lerch, K.; Winkler, M. E.; Solomon, E. I. *J. Am. Chem. Soc.* **1985**, *107*, 4015−4027.
(8) Op't Holt, B. T.; Vance, M. A.; Mirica, L. M.; Heppner, D. E.; Stack, T. D. P.; Solomon, E. I. *J. Am. Chem. Soc.* **2009**, *131*, 6421−6438.
(9) Matoba, Y.; Kumagai, T.; Yamamoto, A.; Yoshitsu, H.; Sugiyama, M. *J. Biol. Chem.* **2006**, *281*, 8981−8990.
(10) Cassidy, A.; Hanley, B.; Lamuela-Raventos, R. M. *J. Sci. Food Agric.* **2000**, *80*, 1044−1062.
(11) Frémont, L. *Life Sci.* **2000**, *66*, 663−673.
(12) German, J. B.; Walzem, R. L. *Annu. Rev. Nutr.* **2000**, *20*, 561−593.
(13) González Ureña, A.; Orea, J. M.; Montero, C.; Jiménez, J. B.; González, J. L.; Sánchez, A.; Dorado, M. *J. Agric. Food Chem.* **2003**, *51*, 82−89.
(14) Pervaiz, S. *Drug Resist. Updates* **2004**, *7*, 333−344.
(15) Savouret, J. F.; Quesne, M. *Biomed. Pharmacother.* **2002**, *56*, 84−87.
(16) Soleas, G. J.; Diamandis, E. P.; Goldberg, D. M. *Clin. Biochem.* **1997**, *30*, 91−113.
(17) Gilly, R.; Mara, D.; Oded, S.; Zohar, K. *J. Agric. Food Chem.* **2001**, *49*, 1479−1485.
(18) Millo, D.; Bonifacio, A.; Ranieri, A.; Borsari, M.; Gooijer, C.; van der Zwan, G. *Langmuir* **2007**, *23*, 9898−9904.
(19) Bonifacio, A.; Millo, D.; Keizers, P.; Boegschoten, R.; Commandeur, J.; Vermeulen, N.; Gooijer, C.; van der Zwan, G. *J. Biol. Inorg. Chem.* **2008**, *13*, 85−96.
(20) Brandt, N. N.; Brovko, O. O.; Chikishev, A. Y.; Paraschuk, O. D. *Appl. Spectrosc.* **2006**, *60*, 288−293.
(21) Pinto, M.; Garcia-Barrado, J.; Macias, P. *J. Agric. Food Chem.* **2003**, *51*, 1653−1657.
(22) Madani, W.; Kermasha, S.; Versari, A. *J. Agric. Food Chem.* **1999**, *47*, 2486−2490.
(23) Richard-Forget, F. C.; Rouet-Mayer, M. A.; Goupy, P. M.; Philippon, J.; Nicolas, J. J. *J. Agric. Food Chem.* **1992**, *40*, 2114−2122.
(24) Root, D. E.; Mahroof-Tahir, M.; Karlin, K. D.; Solomon, E. I. *Inorg. Chem.* **1998**, *37*, 4838−4848.
(25) Baldwin, M. J.; Root, D. E.; Pate, J. E.; Fujisawa, K.; Kitajima, N.; Solomon, E. I. *J. Am. Chem. Soc.* **1992**, *114*, 10421−10431.